Assessing the effects of luminescently labelled and non-labelled PET nanoparticles on environmental bacteria

Klaudia Krysiak-Smułek[1], Wojciech Smułek[2], Dominika Przybylska[1], Zbigniew Hnatejko[1], Ewa Kaczorek[2], Tomasz Grzyb[1*]

[1] *Department of Rare Earths, Faculty of Chemistry, Adam Mickiewicz University, Poznań, Uniwersytetu Poznańskiego 8, 61-614 Poznań, Poland*

[2] *Institute of Chemical Technology and Engineering, Faculty of Chemical Technology, Poznan University of Technology, Berdychowo 4, 60-965 Poznań, Poland*

*corresponding author e-mail: tgrzyb@amu.edu.pl

Abstract

Manufacturers use polyethylene terephthalate (PET) to create many everyday objects, which break down into nanoparticles when released into the environment. This fact raises questions about the effects of nanometric PET on living organisms, including bacteria. However, studies on nanoPET are rare and challenging, even if only because its detection and visualisation are difficult. We studied nanoPET toxicity on selected bacteria and tested its visualisation in biological samples using three nanoPET types: pure, labelled with upconverting nanoparticles (UCNPs), and labelled with Eu^{3+} complex compound. The resulting colloids were characterized using dynamic light scattering, zeta potential, and emission measurements. The results confirmed the development of a method for preparing a stable aqueous colloid of nanoPET. Toxicity tests on *Bacillus*, *Lelliottia*, and *Pseudomonas* strains were carried out using the AlamarBlue method, along with measurements of Glutathione S-Transferase enzyme activity. The impact of labelled and non-labelled nanoPET on bacterial carbon utilisation of different sources was also evaluated. Crystal violet and the *o*-nitrophenyl-β-D-galactoside assays were applied to assess changes in membrane permeability. The adhesion of nanoPET to bacterial cells was examined using atomic force microscopy, and biofilm alterations were visualised under an optical microscope. UCNPs enabled the detection of nanoPET aggregation in bacterial biofilms. PET nanoparticles had a neutral or stimulating effect on bacterial growth. Cell membrane permeability varied depending on the bacterial strain and the type of nanoPET used. The results offer valuable insight into the environmental impact of nanoPET and demonstrate the effectiveness of the new nanoplastic labelling and detection method.

Keywords: *polyethylene terephthalate, nanoplastics, UCNPs, europium, bacteria, bioimaging, toxicity*

1. Introduction

Polyethylene terephthalate (PET) is one of the most widely used compounds for producing plastics. It is used to make bottles for beverages (Benyathiar et al., 2022), packaging for food (Dhaka et al., 2022), fibres for the textile industry (Sulyman et al., 2016), photographic films (Singh et al., 2021), feedstock for 3D printing (Nwogu et al., 2019), or plastic composites for automotive applications (Owen et al., 2022). PET items are exposed to weathering, mechanical abrasion, and slow decomposition, forming micro- and nanoplastics (Karkanorachaki et al., 2022). The latter ranges in size from 1 nm to 1 μm (European Commission. Directorate General

for Environment. and University of the West of England (UWE). Science Communication Unit., 2023). Nanometric PET particles (nanoPET) have been found in the air (Ortega and Cortés-Arriagada, 2023), soil (Bläsing and Amelung, 2018) and water (Cortés-Arriagada, 2021), where they interact with different macro- and microorganisms such as bacteria.

Given the high prevalence of PET objects, the question arises of how nanometric PET affects the environment and human health. Djapovic et al. performed toxicity tests on 11 different compounds, such as PET powder blocks or PET degradation products (Djapovic et al., 2021). They conducted the tests on a selected strain of murine bacteria and human lung cells. They demonstrated that some of these compounds proved to be toxic. Piccardo et al. showed in their work that the presence of micrometric PET negatively affects the growth of echinoderms (*Paracentrotus lividus*) larvae and found no toxic effects of micrometric PET on bacteria of the species *Vibrio fischeri* and algae (*Phaeodactylum tricornutum*) (Piccardo et al., 2020). Sathicq et al. investigated the effect of microplastic PET on the growth of pathogens present in water reservoirs. They demonstrated that the presence of microplastics influenced the agglomeration of microorganisms. Furthermore, microPET supported the maintenance of the tested pathogens in water reservoirs and did not significantly affect their growth (Sathicq et al., 2022). To date, there is little research on the environmental impact of nanoPET.

A challenge that scientists have been facing recently is the detection of plastics in biological materials. Like other plastics, PET is an organic compound of chemical and elemental composition similar to the matter of biological origin. Bacteria are made of organic compounds, so traditional techniques for analysing organic compounds cannot distinguish between plastic and biological material (Bläsing and Amelung, 2018). One solution to this problem may be to label nanoPET with photon upconverting nanoparticles (UCNPs).

The photon upconversion phenomenon is the ability of materials to absorb radiation of lower energy and emit radiation of higher energy (Auzel, 2004). In this way, acting with radiation from the near-infrared (NIR) range, typically with a wavelength of 975 nm, can produce light emission from the visible or ultraviolet range (Jurga et al., 2023). Biological materials, including bacteria, do not exhibit emissions under the NIR radiation (Jin et al., 2017). Hence, it is possible to observe the emission signal from UCNPs-labelled materials without the autofluorescence of biomaterials (Mettenbrink et al., 2022). Additionally, the NIR radiation is usually much less harmful to the biological sample than ultraviolet or visible light. UCNPs, because of their inorganic composition, are chemically stable and resistant to photobleaching, which makes them ideal candidates for labels.

Another way to detect nanoplastics in biological materials could be labelling them with fluorescent dyes showing emission under typical excitation sources used in microscopy from the 375 – 450 nm range. Dyes, because of their organic structure, are expected to penetrate and mix better with the polymer structure. However, such excitation wavelengths can produce autofluorescence of biomaterial, which makes distinguishing the emission of plastics from the emission of biomaterial difficult. A good solution to the difficulties with using dyes is to use the emission of europium ions at their +III oxidation state (Eu^{3+}). Compounds containing Eu^{3+} ions usually generate a red emission, with narrow bands at around 580 and 615 nm, when irradiated in the ultraviolet/blue range (Grzyb and Lis, 2011; Szczeszak et al., 2016). The large Stokes shift allows for better visualisation of Eu^{3+}-based emission from the autofluorescence of biomaterials, typically occurring in the blue and green spectral range. Jannatin et al. developed

a method for trapping and detecting bacteria by mixing them with Eu^{3+} ions and then performing fluorescence spectroscopy (Jannatin et al., 2024). The emission spectra they obtained show signals characteristic of Eu^{3+} ions, which means that the autofluorescence of the bacteria does not interfere with the detected emission. However, the toxicity of the Eu^{3+} compounds may be a potential problem (Pallares et al., 2021).

Various methods for obtaining and testing nanoPET have been described in the literature, including labelled PET. Johnson et al. described the preparation of rhodamine B-labelled nanoPET, but the colloid they prepared was suspended in a 0.5 mg/mL BSA solution, which could affect the way in which nanoPET interacted with the studied cells (Johnson et al., 2021). Since, in nature, most often, water is a dispersant and transporter of substances that are absorbed by microorganisms, it would be best to obtain a nanoPET colloid dispersed in pure water. An aqueous colloid of unlabelled nanoPET was obtained by Sharma et al. (Sharma et al., 2024). The described process involves the use of not only hexafluoroisopropanol but also toluene and sodium cholate. The method we developed allows for a more straightforward way to obtain a stable aqueous nanoPET colloid without using complex and chemical-consuming procedures.

The aim of the study was to test the effects of labelled and unlabelled nanometric PET on selected bacterial strains and to check whether nanoPET is absorbed into the bacterial biofilm. This paper describes an innovative method for obtaining a stable aqueous nanoPET colloid and its characterisation. The present study also responds to the problem of bioimaging nanoPET in biological materials. In this publication, we present an innovative way to obtain nanoPET labelled with UCNPs, which enabled nanoPET to be bioimaged in a bacterial biofilm. All nanoPETs obtained in the publication were also subjected to ecotoxicity tests on three strains of environmental bacteria. Concentration-dependent nanoPET toxicity and membrane permeation tests were performed. In addition, it was examined how the presence of nanoPET affects the utilisation of carbon by bacteria from different sources. Moreover, the adhesion of labelled and unlabelled nanoPETs to the bacterial surface was investigated by AFM, which, according to our literature review, has never been published before. However, the most groundbreaking study is the imaging of nanoPET labelled with UCNPs in a bacterial biofilm, which confirms that a method has been discovered to distinguish the labelled nanoplastic from the bacterial biomass.

2. Materials and methods

2.1 Materials

The PET pellets used in the study were produced by UAB NEO GROUP (Lithuania). Hexafluoroisopropanol (HFIP) was purchased from Fluorochem Ltd (UK). A Spectra/Por 1 dialysis membrane from Spectrum Laboratories Inc (USA) was used. All salts and indicators, like crystal violet (CV), *o*-nitrophenol-β-galactoside (ONPG), and Glutathione S-Transferase (GST) assay kit, used in the microbiological tests, were purchased from Merck (Germany). AlamarBlue was provided by PolAura (Poland). The culture media, like nutrient broth, were sourced from BTL Sp. z o.o. (Poland). Oleic acid (extra pure, Fisher Scientific), 1-octadecene (technical grade 90 %, Alfa Aesar), ammonium fluoride (min. 98.0 %, Alfa Aesar), sodium oleate (82 %, Sigma Aldrich), acetic acid glacial (99.5% POCH S.A), acetic acid (80% POCH S.A), yttrium(III) acetate tetrahydrate (99.9 %, Alfa Aesar), ytterbium oxide and erbium oxide (99.9 %, Stanford Materials), hydrochloric acid extra pure (ultra-pure, Sigma-Aldrich, 37%, Poland), *n*-hexane (95%, VWR Chemicals), ethanol (98.8 %, POCH S.A.), and demineralised

water without any further purification. 2-thenoyltrifluoroacetone and europium(III) chloride were purchased from Sigma-Aldrich.

2.2 Preparation of the polyethylene terephthalate nanosized particles (nanoPET)

2.2.1 NanoPET

To obtain an aqueous nanoPET solution, the method described by (Johnson et al., 2021) was modified. A schematic of the modified synthesis is shown in Figure 1. PET pellets were dissolved in HFIP for a 15 mg/mL solution. The system was maintained at 45°C until complete dissolution. The resulting PET solution in organic solvent was dropped into a stirred distilled water at 59°C (boiling point of HFIP). An automatic syringe pump NE-1000 (New Era Pump Systems Inc., Farmingdale, NY, USA) dropped the PET solution at a rate of 50 µL/min. The mass ratio of PET to water was 1:2285. A homogeneous, iridescent colloid was obtained.

2.2.2 NanoPET labelled with UCNPs

NanoPET labelled with UCNPs (nanoPET+UCNPs) was prepared analogously to the unlabelled one. The core@shell UCNPs were obtained according to the procedure described in the Supplementary Materials. A solution of PET in HFIP (15 mg/mL) was mixed and ultrasonicated with a colloidal solution of UCNPs (31 mg/mL), keeping the mass ratio of 4:1. The resulting mixture was then injected under the same conditions as the unlabelled nanoPET.

2.2.3 NanoPET labelled with Eu^{3+} complex compound

The method of obtaining $Eu(TTA)_3$ (TTA = 2-thenoyltrifluoroacetonate) is described in the Supplementary Materials. A solution of $Eu(TTA)_3$ in HFIP was prepared with a concentration of 1 mg/mL. NanoPET labelled with Eu^{3+} complex compound (nanoPET+$Eu(TTA)_3$) was obtained analogously to those described above. The PET and $Eu(TTA)_3$ solutions were mixed in a mass ratio of 59:1 and then ultrasonicated. Thus, the mixture obtained was infused into water under the same conditions described above.

2.2.4 Purification

Each prepared nanoplastic colloid was purified from HFIP and, in the case of nanoPET+UCNPs, also from hexane. The purification process consisted of membrane dialysis and took 72 hours. The efficiency of the purification process was checked by performing IR spectra of the suspension (Figure S5) using the Vertex 70 (Bruker, Germany) Spectrometer equipped with a MIRacle™ ATR accessory (single reflection diamond ATR crystal). There are no peaks on the spectra indicative of the presence of these solvents. This demonstrates the efficiency of the purification process.

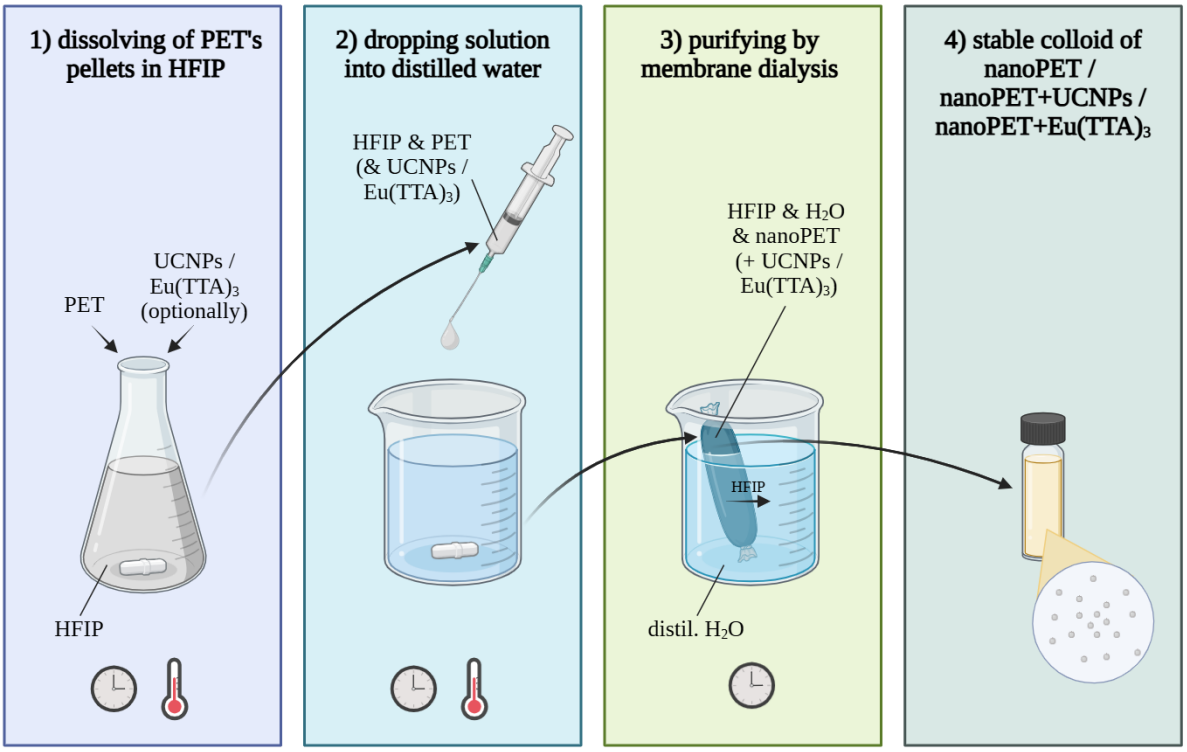

Figure 1. Scheme of the nanoPET, nanoPET+UCNPs, and nanoPET+$Eu(TTA)_3$ synthesis.

2.3 Analytical methods

Spectroscopic characterisation of the $Eu(TTA)_3$ complex, $NaYF_4$:18%Yb^{3+},2%Er^{3+}@$NaYF_4$ UCNPs, and labelled nanoPET – either as colloids or in solution (Eu^{3+} complex) – was performed at room temperature. A fibre-coupled CNI 2W continuous-wave 975 nm solid-state diode-pumped (SSDP) laser or a 375 nm continuous-wave UV SSDP laser, along with a PIXIS:256E digital CCD camera and an SP-2156 imaging spectrograph (Princeton Instruments), were used for spectra measurements. The beam size and laser powers were determined using a 10A-PPS power meter (Ophir Photonics). Zetasizer Nano was used to check the hydrodynamic diameter of the nanoparticles in the resulting colloids at 25°C using backward scattering (173°) (Malvern Instruments Ltd, Malvern, UK). The polydispersity index (PDI) and zeta potential were determined using the same device.

2.4 Bacteria assays

2.4.1 Introduction of nanoplastics for the cultivation of environmental bacteria

Three bacterial strains isolated from environmental samples were used in this study, whose taxonomic affiliation was determined by comparison of 16S RNA sequences: *Bacillus thuringiensis* KlaKry (NCBI GenBank No. PP594216), *Lelliottia nimipressuralis* KlaKry (NCBI GenBank No. PP596117), *Pseudomonas plecoglossicida* IsA (NCBI GenBank No. KY561350). These three strains were isolated from environmental samples and described in previous publications (Smułek et al., 2019; Sroczyńska et al., 2024), were selected and represent different types of bacteria typically found in aquatic ecosystems, allowing a more diverse perspective to assess the impact of nanoPET on bacteria. Bacterial inoculum was prepared in the nutrient broth by incubating the cultures for 24 h at 30°C. After this time, the biomass was

washed with fresh medium or PBS buffer, standardised for optical density at 600 nm (equal to 0.5) and then mixed with a suspension of nanoPET (labelled or unlabelled) in PBS, taking care to ensure the desired nanoPET concentration and constant ionic strength (to avoid osmotic shock) in the test systems. All microbiological tests described in the following section were performed after a twenty-four-hour exposure to nanoPET (unless otherwise stated in the method description). Abiotic tests (without bacteria) and control tests (without any nanoPET) were performed for all experiments.

2.4.2 Toxicity measurements

The AlamarBlue® assay (Thermo Fisher Scientific, Waltham, MA, USA) was applied to evaluate bacteria viability in the presence of nanoPET. The control sample was cultured without the addition of nanoPET. Fluorescence was measured using a GloMax (Promega, Walldorf, Germany) device at a 580–640 nm wavelength range. Carbon substrate utilisation patterns (after 24 h, 48 h, 72 h, and 168 h) were determined using a commercial phenotyping microarray tool (Biolog EcoPlate™ Inc., Hayward, CA, USA) (Sofo and Ricciuti, 2019). For each bacteria+nanoPET combination, one EcoPlate (each with three replications of the same carbon source set) was used for a specific concentration of nanoPET. Moreover, the impact of nanoPET (100 mg/L) on microbial glutathione S-transferases (GST) activity was investigated. The cells from 48h-cultures were washed and lysed using the CelLytic™ B Plus Kit (Sigma-Aldrich, Germany). The bacterial lysates were used to measure total GST using a Glutathione S-Transferase Assay Kit (Sigma Aldrich, MO, USA), which utilises 1-Chloro-2,4-dinitrobenzene (CDNB). Upon conjugation of the thiol group of glutathione to the CDNB substrate, an increase in the absorbance at 340 nm was observed, measured with a Multiskan Sky Microplate Spectrophotometer (Thermo Fisher Scientific, Agawam, MA, USA) (Smułek et al., 2020).

2.4.3 Effects on cell membrane permeability

Inner membrane permeability was further assessed using the *o*-nitrophenyl-β-D-galactoside (ONPG) assay, which measures the concentration of *o*-nitrophenyl (a product of ONPG hydrolysis catalysed by β-galactosidase – enzyme released from the bacteria cells) (Pacholak et al., 2018). Total membrane permeability was evaluated through the crystal violet (CV) uptake assay, which relies on colourimetric analysis of dye absorption by microbial cells (at 590 nm) (Devi et al., 2013).

2.5 Bioimaging

Further studies focused on the analysis of the incorporation of nanoPET into the bacterial biofilm formed by the bacterial strains being screened out. The test consisted of placing 200 µL of the cell suspension together with the nanoPET (100 mg/L) prepared as described in section 2.4.1 in wells of a 96-well polystyrene plate. After 48 h of incubation, the solution was pipetted out of the well without disturbing the biofilm formed at the bottom. Bacterial biofilms exposed to the nanoplastics were viewed under a digital microscope VHX-6000 (Keyence, Osaka, Japan). The analysis with the multimode plate reader (Uniogen, Turku, Finland) was carried out to show that the UCNPs-labelled nanoplastic had been absorbed by the bacterial biofilm. To confirm the presence of the nanoPET+$Eu(TTA)_3$ in the bacterial biofilm, the biomass was mixed with 100 µL of 10% NaOH, left overnight, and mixed with 100 µL of deionised water. Then, nanoPET+$Eu(TTA)_3$ were investigated using a GloMax (Promega, Walldorf, Germany)

device. Moreover, an atomic force microscope (AFM), Park NX10 (Park Systems Corp., Suwon, Korea), was used for observations of nanoPETs' interaction with bacteria cells.

2.6. Statistical analysis

All measurements were conducted in triplicate, and for each measurement set, arithmetic mean, standard deviation, and statistical error were calculated. Statistical significance between the means of each independent measurement set in each experiment was assessed using analysis of variance (ANOVA), with the Tukey HSD test as a post-hoc test and *p*-value less than 0.05. Lowercase letters on the graphs indicate statistically significant differences among the results within the results series. All statistical analyses were performed using Microsoft Excel 2013 and Origin Pro (OriginPro 2025 (64-bit) SR1), which was also used to prepare the graphs.

3. Results

3.1 Characterisation of the nanoPETs

3.1.1 DLS, PDI, and zeta potential

The described synthesis methods enabled the production of stable, iridescent nanoplastic colloids. DLS analysis was performed to check the size of the resulting nanoplastics. The hydrodynamic diameter measurement of nanoPET (Figure S6A) showed a result of 115.4±32.4 nm (Z-Average 143.1 nm, PdI 0.048, zeta potential -33.9±8.0) for nanoPET+UCNPs (Figure S6B), a result of 117.7±39.9 (Z-Average 159.4, PdI 0.118, zeta potential -39.0±11.2), while for nanoPET+$Eu(TTA)_3$ (Figure S6C), 144.2±41.9 (Z-Average 172.7, PdI 0.063, zeta potential -30.3±7.3). The DLS technique confirmed that the PET colloids contain nanometric particles with a size not exceeding 150 nm. The nanometric size of the prepared nanoPETs was also confirmed by AFM images (Figure 6). The zeta potential measurement showed that all the PET particles obtained were negatively charged. The labelling dopants were neutral for the nanoPET sizes or zeta potentials.

The supplementary materials include additional characterisation results, such as DLS data for the UCNPs (Figure S1), TEM images (Figures S2A–B), and size calculations of the UCNPs based on these images (Figure S2C). According to the analyses, the diameter of the UCNPs used for plastic labelling was 46.5±10.7 nm. DLS analysis of nanoPET+UCNPs did not reveal the presence of such small nanoparticles in the nanoplastic colloid, suggesting that all UCNPs were incorporated into the resulting nanoPET structure.

Figure S3 and Figure S4 illustrate X-ray diffraction spectra (XRD) of the UCNPs and nanoplastic, respectively. XRD analysis confirms the successful synthesis of UCNPs – hexagonal β-$NaYF_4$ was obtained. The XRD patterns of the UCNPs-labelled nanoplastic confirmed the presence of a small amount of inorganic nanoparticles in the structure of nanoPET. The peaks at around 31° and 43° 2 theta coincide with the pattern lines, but they are of low intensity due to the high level of background signal.

3.1.2 Spectroscopic properties

Some of the lanthanide ions (Ln^{3+}), such as Tb^{3+}, Sm^{3+}, or Eu^{3+} ions, show luminescence when exposed to radiation from the ultraviolet to NIR range, depending on the mechanism of excitation (Jurga et al., 2025; Przybylska et al., 2024). Examples of Ln^{3+} ions emissions are presented in Figures 2A, C (emission of Er^{3+} ions under 975 nm excitation) and Figures 2B, D (emission of Eu^{3+} ions under 375 nm excitation).

The ability of Ln^{3+} ions to present emission is related to the specific nature of the inner 4f subshell electrons and their isolation from the surrounding environment by the outer 5s and 5p subshells. Thanks to this structure, electrons from the 4f shell interact weakly with the environment and do not participate in chemical reactions (Mallah et al., 2008). However, the most important thing is that the shielding effect of the 5s and 5p electrons results in a ladder-like structure of Ln^{3+} energy levels, which is typical for each ion's narrow emission bands. Figure 2 shows the spectra of Er^{3+} and Eu^{3+} ions with narrow emission lines in the green (Er^{3+}) or red (Eu^{3+}) spectral ranges. Besides the emission characteristics, the electronic structure of the Ln^{3+} ions enables complex energy transfer processes, such as upconversion phenomena (Auzel, 2004; Jurga et al., 2022).

In the following work, we present two types of Ln^{3+} ions emission: photon upconversion (Figure 2A, C) and downshifted luminescence (Figure 2B, D). Thanks to this, we can compare how these two types of luminescence can be used in the visualisation of the labelled nanoPET.

UCNPs used in our experiments were core@shell $NaYF_4$ structures doped with Yb^{3+} and Er^{3+} ions. Typically, UCNPs are inorganic matrices doped with optically active Ln^{3+} ions that can sequentially absorb two or more photons and convert them into a smaller number of photons with higher energy than those originally absorbed. The most efficient upconverting systems operate via the energy transfer upconversion (ETU) mechanism (Würth et al., 2022), used in our research, in which two Ln^{3+} ions—either identical or different—function as a sensitiser and an emitter. The sensitiser absorbs the excitation light and transfers the energy to the emitter. In the emitter, this energy promotes Ln^{3+} ions to their higher excited states, from which light is subsequently emitted.

The used in our studies β-$NaYF_4$ nanoparticles doped with Yb^{3+} and Er^{3+} ions, are one of the most effective systems for the upconversion process. Yb^{3+} ions are excellent sensitisers because they can store energy due to their long luminescence decay time. Er^{3+} ions, on the other hand, show efficient anti-Stokes emission with major emission bands at 520, 545, and 660 nm and are good emitters. The intensity of upconversion of the studied nanoparticles was additionally strengthened by synthesising core@shell structures, where the shell protects the luminescent core from quenching of surface-related factors. UCNPs constructed in this way show much higher fluorescence than known fluorescent substances such as fluorescein or rhodamine 6G (Misiak et al., 2012).

Downshifting, or Stokes-like emission, is a process in which excitation by high-energy radiation, typically in the ultraviolet range, results in light emission with an energy lower than that of the pumping radiation (Sun et al., 2021). Because Ln^{3+} ions show relatively weak radiation absorption in solution, their complexes are usually used if the emission intensity is important. The ligands of the chelating compound absorb UV radiation and transfer the absorbed energy to the Ln^{3+} ion coordinated with them, which emits light. Of the rare earth elements, Eu^{3+} ions were chosen for the study because of their luminescent properties and beneficial energy level structure (Prabakaran and Pillay, 2020). TTA ligands effectively transfer the absorbed energy to the Eu^{3+} ion due to the similarity between the energy of Eu^{3+} at higher excited levels and the energy of the TTA triplet state (Brennetot and Georges, 2000).

Figure 2 shows the studied systems' emission spectra and pictures of their emission in the form of solutions or colloids. The UCNP (Figure 2A) and nanoPET+UCNP (Figure 2C) colloids exhibit emission bands characteristic of Er^{3+} ions, corresponding to transitions from the $^2H_{11/2}$,

$^4S_{3/2}$, and $^4F_{9/2}$ excited states to the $^4I_{15/2}$ ground state, observed at 520, 545, and 660 nm, respectively. The nanoPET labelled with UCNPs shows lower emission intensity, which is attributed to the dilution of nanoparticles within the PET matrix and scattering of the excitation light. As upconversion is a non-linear process, the scattering lowers the power density of the NIR excitation radiation, dramatically reducing the intensity of UCNPs emission.

$Eu(TTA)_3$ complex solution and $Eu(TTA)_3$-labelled nanoPET presented emission bands under 375 nm excitation light, related to the transitions from the $^5D_0$ excited state of Eu^{3+} ions to the components of the ^7F_J ground state (J = 1 – 4) of this ion. The main emission peaks were detected at 588, 612, 647, and 693 nm. The emission of the Eu^{3+} containing nanoPET is more intense in contrast to the UCNPs-labelled ones, which is also connected with scattering, but, in this case, of the emission light, not excitation.

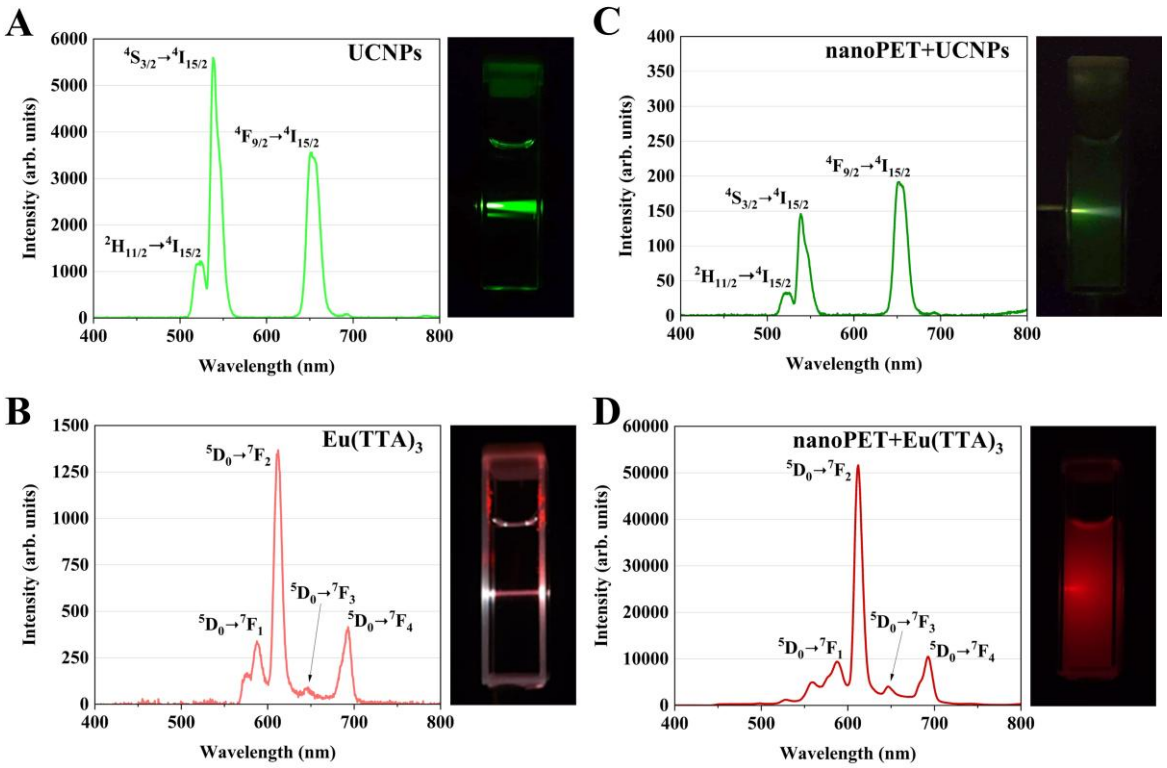

Figure 2. Emission spectra and photographs of UCNPs (A) and nanoPET+UCNPs (C) colloids under 975 nm laser excitation (26 W/cm^2). In both samples, the UCNPs concentration was 100 µg/mL, corresponding to a nanoPET concentration of 400 µg/mL in the labelled system. Panels (B) and (D) show the emission spectra and images of $Eu(TTA)_3$ and nanoPET+$Eu(TTA)_3$ colloids under 375 nm laser excitation (1 W/cm^2). The $Eu(TTA)_3$ concentration was 8 µg/mL in both colloids, corresponding to a nanoPET concentration of 472 µg/mL in the labelled sample.

3.2 Bacteria results

3.2.1 Toxicity and changes in bacterial metabolism

The toxicity of labelled and unlabelled nanoPET was tested using the AlamarBlue method. For better clarity of the results presentation, bacterial growth is given in relative values, taking the mean of the measurements for the control sample (without nanoPET) to be 1.0. The values for the other measurement series (with a given nanoPET concentration) were converted

proportionally to the control sample. The results summarised in Figure 3A show that the presence of nanosized PET had a stimulating effect on *Bacillus* growth. For all PETs tested, the biggest growth of *Bacillus* was obtained for the highest concentrations. A significant increase in bacterial growth was observed at the lowest tested concentration of the nanoPET+Eu(TTA)$_3$.

In the case of the *Lelliottia* strain (Figure 3B), all tested nanoPETs positively affected the growth of bacteria. The highest concentration of labelled and non-labelled nanoPETs caused the most pronounced increase in bacterial growth. Bacteria of the genus *Pseudomonas* showed a greater increase in growth in the presence of unlabelled nanoPETs, whereas no significant differences were observed when exposed to labelled nanoPETs (Figure 3C).

Although a stimulatory effect or no effect of nanoPETs on bacterial cell growth was observed, measurement of GST activity showed that each strain had to use GST to detoxify each nanoPETs tested. For *Bacillus* (Figure 3D) and *Lelliottia* (Figure 3E), the most significant loss of enzyme activity was observed in the presence of nanoPET+UCNPs, while slightly less was observed with the other two nanoPETs. The results for the *Pseudomonas* strain (Figure 3F) show the opposite trend, *i.e.,* the most significant decrease in GST activity was registered for *Pseudomonas* in the presence of nanoPET and nanoPET+Eu(TTA)$_3$. In contrast, a slightly less intense reduction in activity was observed with nanoPET+UCNPs.

Additional information on the utilisation of carbon sources by bacteria in nanoPETs was provided by tests on EcoPlates (Figure 4). At Tween 80, strains *Bacillus* and *Pseudomonas* showed greater growth in the presence of each nanoPET type than the control. For glycogen assimilation by *Lelliottia*, it was observed that nanoPETs had a neutral effect, nanoPET+UCNPs caused a decrease, while nanoPET+Eu(TTA)$_3$ increased bacterial growth. With D-cellobiose, *Bacillus* growth was reduced in the presence of all nanoPETs tested. An apparent reduction in the growth of *Pseudomonas* on β-methyl-D-glucoside was observed with the addition of each PET, with the most pronounced effect seen for nanoPET+Eu(TTA)$_3$. Both *Bacillus* and *Lelliottia* from nanoPET+UCNPs on D-mannitol grew much better than in samples with the other nanoPETs and the control.

In contrast, both strains grew better on N-acetyl-D-glucosamine without plastic and at least well with nanoPET and nanoPET+Eu(TTA)$_3$. For *Lelliottia* with glucose-1-phosphate, the best growth was observed with nanoPET+UCNPs. No growth was observed on alpha-ketobutyric acid, although *Bacillus* and *Pseudomonas* with nanoPET+UCNPs showed gentle growth after one week (168 h). *Bacillus* and *Lelliottia* on L-phenylalanine substrate showed growth in the presence of nanoPET and nanoPET+UCNPs, while *Pseudomonas* additionally also showed growth in the presence of nanoPET+Eu(TTA)$_3$. On glycyl-L-glutamic acid, the *Bacillus* strain grew more weakly in the presence of nanoPET, while in the presence of labelled nanoPET, the growth was at the same level as the control. With the same carbon source, *Lelliottia* cells grew better in the presence of labelled nanoPETs. At the same time, there is no difference between the culture with nanoPET+UCNPs and the control for *Pseudomonas*, but a weaker growth is observed in the presence of nanoPETs and nanoPET+Eu(TTA)$_3$. No significant differences in bacterial growth were observed with the other carbon sources.

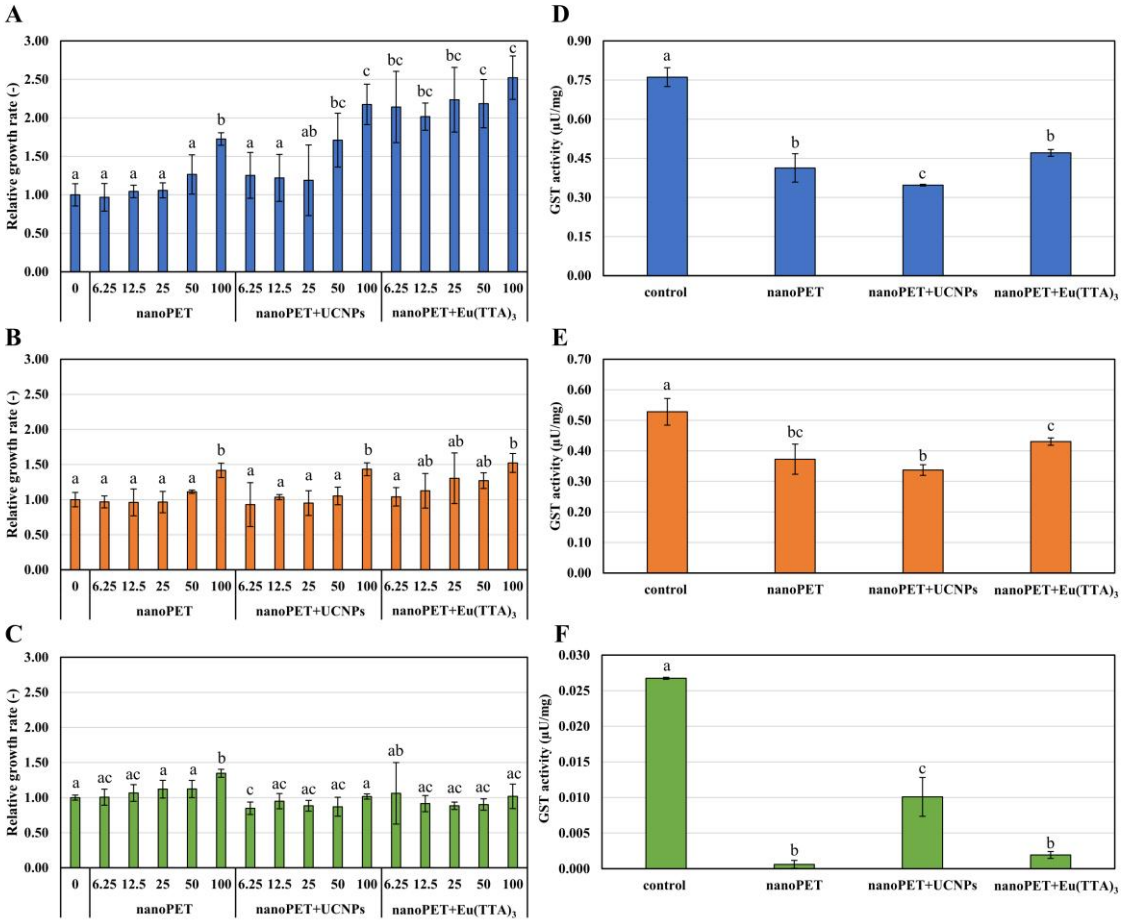

Figure 3. Impact of nanoPET on the growth of bacteria (A-C) and Glutathione S-Transferase activity (D-F) for the strains *Bacillus* (A, D), *Lelliottia* (B, E), *Pseudomonas* (C, F) measured with AlamarBlue assay after 24 h.

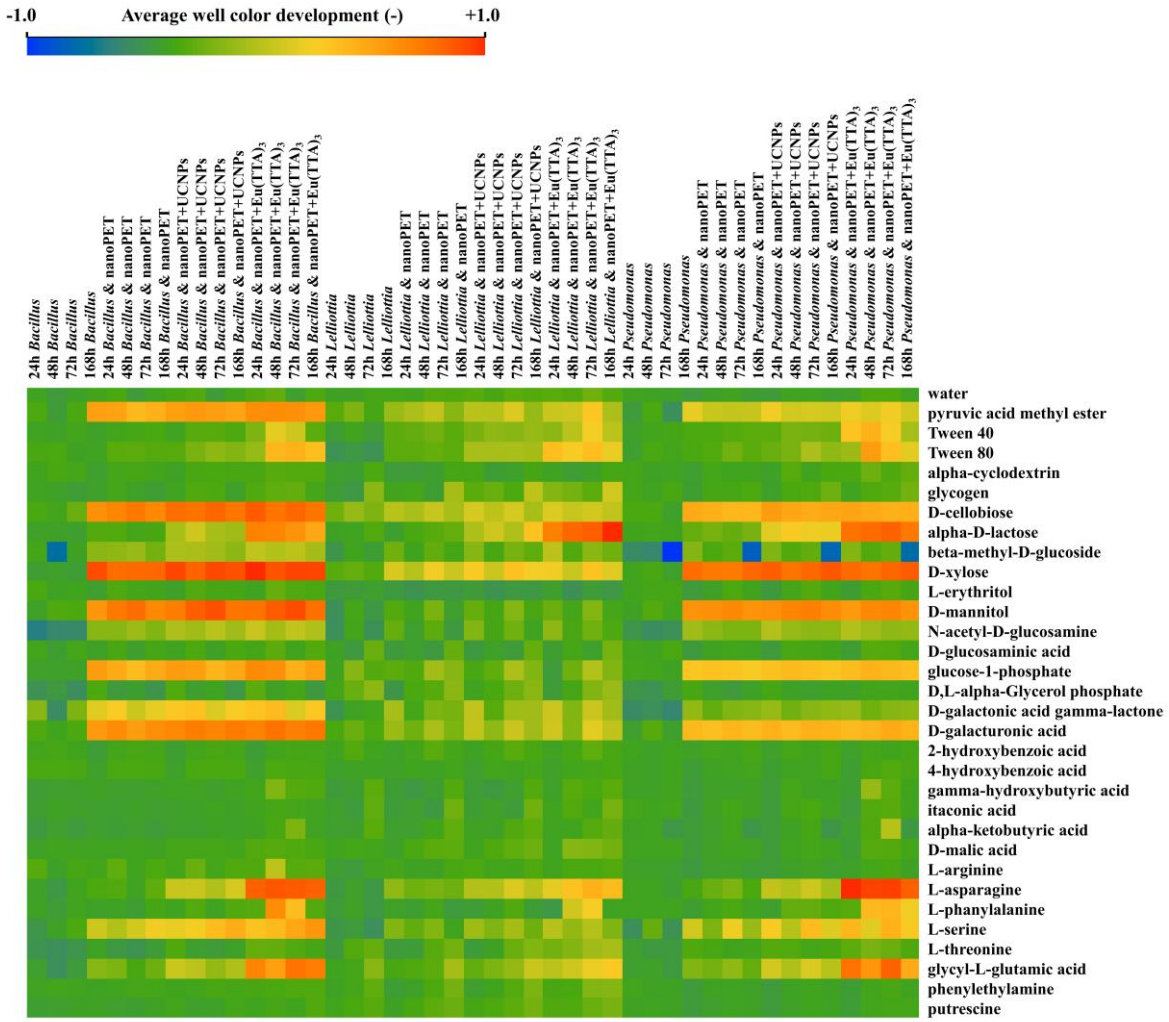

Figure 4. Changes in bacterial utilisation of different carbon sources measured with the EcoPlate assay.

3.2.2. Effects on cell membrane permeability

The changes in bacterial membrane caused by nanoPETs were determined by measuring the crystal violet penetration of the bacterial membrane. Figure 5A shows the penetration of crystal violet through the *Bacillus* membrane in the presence of nanoPETs. An apparent decrease in permeation was only observed at the two highest concentrations of nanoPET+Eu(TTA)$_3$. In the case of *Lelliottia* (Figure 5B), no significant statistical differences in membrane permeability were observed depending on the concentration and type of nanoPET. *Pseudomonas* cell membranes, on the other hand, were more permeable with all concentrations of nanoPET+Eu(TTA)$_3$ (Figure 5C).

The effect of nanoPETs on β-galactosidase release by bacterial cells was investigated using the ONPG assay. *Bacillus* (Figure 5D) and *Lelliottia* (Figure 5E) cells showed a decrease in β-galactosidase enzyme release at higher concentrations of unlabelled nanoPET. For *Pseudomonas* cells (Figure 5F), higher β-galactosidase release (higher permeability) was registered in the presence of lower concentrations of nanoPET+Eu(TTA)$_3$.

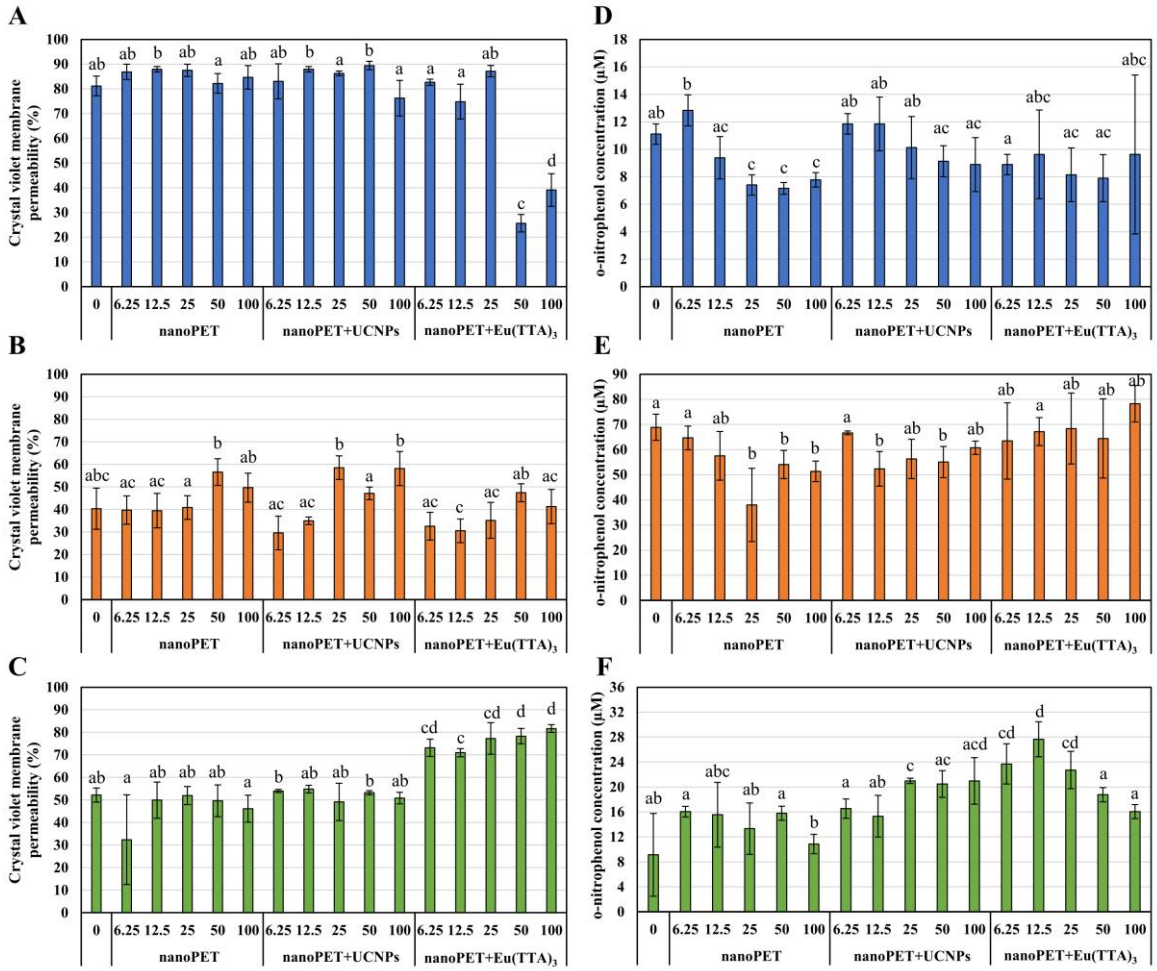

Figure 5. Influence of nanoPET on cell membrane permeability measured with crystal violet assay (A-C) and β-galactosidase release measured by the concentration of *o*-nitrophenol formed by the reaction of the enzyme with ONPG (D-F); results for bacteria from the genera *Bacillus* (A, D), *Lelliottia* (B, E), and *Pseudomonas* (C, F).

3.3. Bioimaging

3.3.1. Microscopy observation

AFM images (Figure 6) confirm the nanometric size of the prepared PET. Besides, they show that nanoPET, nanoPET+UCNPs, and nanoPET+Eu(TTA)$_3$ particles adsorb on the surface of all three tested strains. The obtained PETs agglomerate on the bacterial cells to form long structures. It can be observed that the nanoplastics adhere tightly to bacteria, although they do not uniformly cover the entire cell surface. Also, no damage to bacterial cells was observed in the presence of nanoPETs.

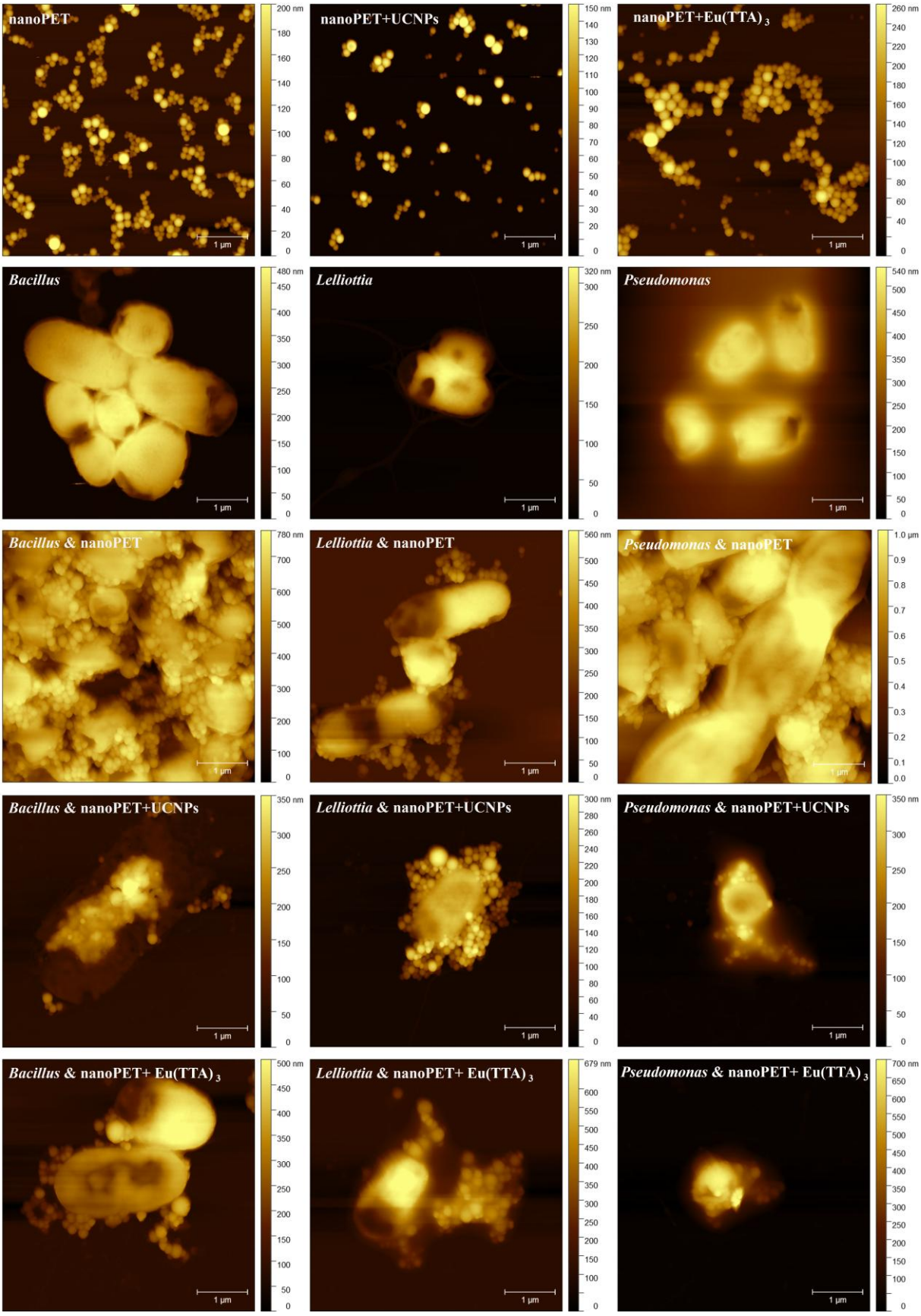

Figure 6. AFM images of nanoplastics, bacteria, and bacteria after exposure to the 100 µg/mL solutions of nanoplastics.

All bacterial strains used in the study showed the ability to form a firm biofilm. Microscopic viewing of the biofilm formed by the bacteria (Figure 7) showed that, in the case of *Pseudomonas*, none of the prepared PET affected biofilm formation. Observation of the biofilm formed by *Bacillus* and *Lelliottia* indicated that nanoPET tends to agglomerate; however, the differences are more subtle in samples with *Lelliottia*. The presence of nanoPET+UCNPs resulted in the formation of agglomerates and nanoPET+Eu(TTA)$_3$, even larger agglomerates.

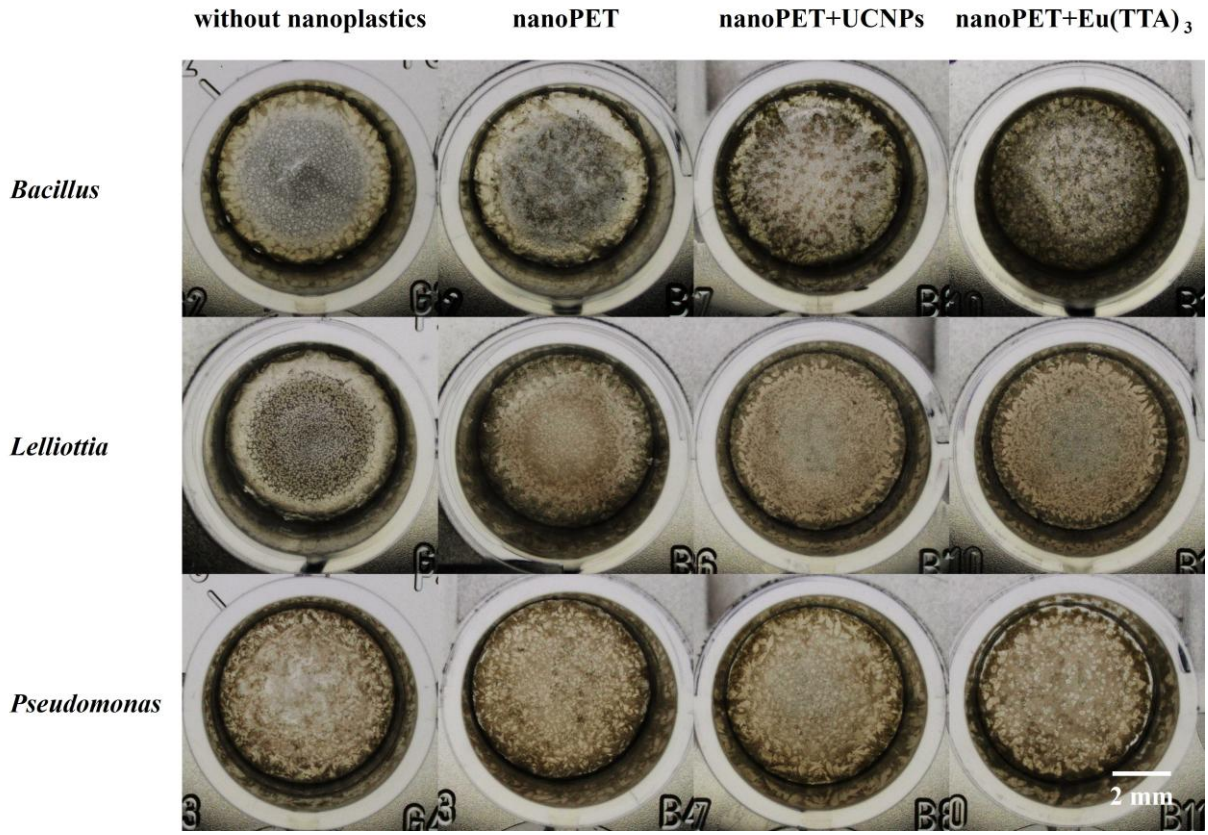

Figure 7. Optical microscopy photographs of the biofilm that the bacteria formed after exposure to the 100 μg/mL solutions of nanoplastics.

3.3.2. Luminescence

The biofilm was analysed using plate readers to determine whether the bacteria had absorbed the nanoPETs during the biofilm formation. The observed differences in the mixed signal intensity ranges for nanoPET labelled with UCNPs and Eu(TTA)$_3$ are due to the different nature of the electromagnetic wave formation (up-conversion vs. fluorescence) and the resulting difference in the measuring instruments used. The results showed that, depending on the concentration of the labelled nanoPET, the bacteria absorbed plastics into their biofilm in different amounts. For nanoPET+UCNPs, imaging was performed (Figure 8A-C). The images show that the nanoPET+UCNPs were not absorbed uniformly. Clusters can be seen near the edges of the wells of the measurement plate. For bacteria without nanoPET+UCNPs, no emission was observed. The results of the tests conducted on solutions formed from biofilms with nanoPET+Eu(TTA)$_3$ are shown in Figure 8D. No trend was observed for either strain. A significant increase in emissions was found at the highest concentration for *Pseudomonas*.

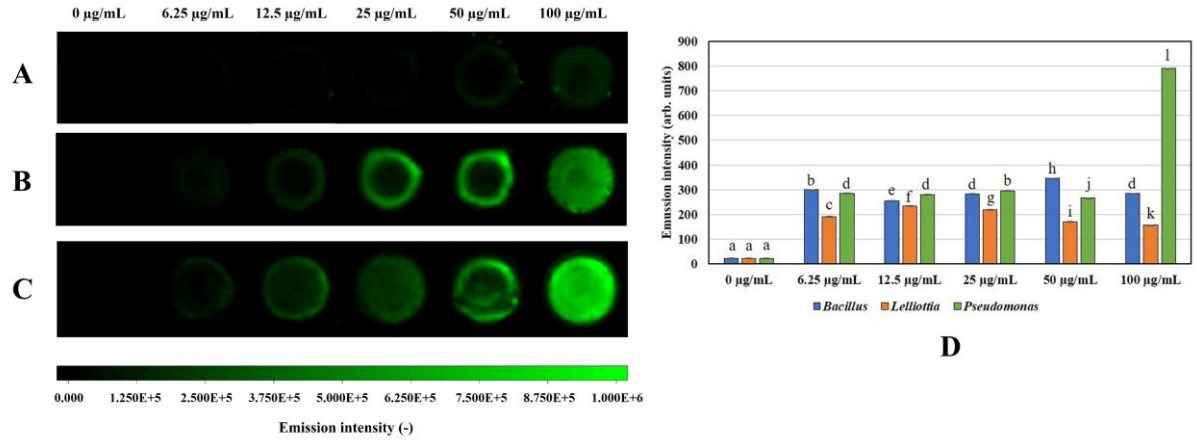

Figure 8. Measurement of emission intensity of labelled nanoPETs adsorbed by bacterial biofilms: nanoPET+UCNPs (A-C) (excitation wavelength of 975 nm, the analysis was performed with the multimode plate reader Uniogen), nanoPET+Eu(TTA)$_3$ (D) (excitation wavelength of 375 nm, the analysis was performed with plate reader GloMax); bacterial strains used: *Bacillus* (A), *Lelliottia* (B), *Pseudomonas* (C).

4. Discussion

The emission spectra of the colloids UCNPs, nanoPET+UCNPs, and nanoPET+Eu(TTA)$_3$ and the Eu(TTA)$_3$ solution confirmed that the prepared nanoPETs contain a suitable indicator, which allows the detection of the nanoplastics by applying upconversion and fluorescence as well. The peaks on the spectra of UCNPs and nanoPET+UCNPs coincide with those for Er^{3+} ions presented by (Pisarski et al., 2017). The signals obtained on the spectra of Eu(TTA)$_3$ and nanoPET+Eu(TTA)$_3$ are the same as those for [Eu(TTA)$_3$(phen)] (phen = 1,10-phenanthroline) in the paper written by (Binnemans, 2015).

The method described for obtaining nanoPET allowed us to obtain a colloid with nanoparticles with a hydrodynamic diameter of 115.4±32.4 nm, which is smaller than that obtained in the publication (Johnson et al., 2021) (170±3 nm). Johnson et al. use a solution of BSA protein at 0.5 mg/mL as a dispersant in the nanoPET colloids, whereas in the colloids prepared by us, the dispersant is distilled water. The same publication describes the preparation of rhodamine B-labelled nanoPET with a hydrodynamic particle diameter of 158±2 nm. Therefore, the labelled nanoPETs we obtained have smaller hydrodynamic diameters. The colloids obtained by Johnson have a slightly lower potential (nanoPET: -37 mV, labelled nanoPET: -38 mV), which means they are also slightly more stable and better dissociated. Nevertheless, what is especially important is that the zeta potential results obtained for our nanoPETs demonstrate that they are stable colloids.

Toxicity tests provided information that unlabelled nanoPET at higher concentrations had a stimulatory effect on each bacterial strain's growth. A similar stimulating effect of nanoPET has been described for the growth of Human Peripheral Blood Mononuclear Cells tested by MTT (Djapovic et al., 2023). Tests were also conducted to evaluate the effect of nanoPET on *E. coli* growth. After 24 h of incubation, no difference in cell growth was observed between samples with and without nanoPET (Sharma et al., 2024). The recorded decrease in GST enzyme activity in the presence of nanoPETs indicates that the bacteria must have taken detoxifying action against the nanoPETs. However, the increase in the number of *Bacillus* and

Lelliottia cells in the presence of all nanoPETs tested, *Pseudomonas* in the presence of unlabelled nanoPET, and the lack of change in *Pseudomonas* cell size with labelled nanoPETs proves that none of the nanoPETs were toxic enough to harm the bacteria. In light of the above observations, it can be assumed that the creation of stress conditions (but at sub-lethal doses) caused by the presence of nanoPET contributes to the stimulation of cell growth. Honselmann Genannt Humme et al. explained similar observations of growth stimulation by ZnO nanoparticles in this way (Honselmann Genannt Humme et al., 2024). It is possible that a similar mutagenic process is occurring here, stimulating the long-term growth of cells resistant to the nanoPET toxin, similar to what Kohanski et al. observed with sub-lethal doses of antibiotics (Kohanski et al., 2010).

Depending on the type of nanoPET and the bacterial strain, increased assimilation of selected carbon sources was observed, such as Tween 80 for *Bacillus* and *Pseudomonas* for all three nanoPETs and alpha-butyric acid for nanoPET+UCNPs. In other cases, nanoPETs decreased carbon assimilation, such as D-cellobiose for Bacillus and N-acetyl-D-glucosamine for *Lelliottia*. In some instances, nanoPETs did not affect carbon assimilation, such as L-asparagine for *Bacillus* and alpha-cyclodextrin for *Lelliottia*. Since no similar study was found for nanoPET, the results obtained were compared with those for polystyrene after 7 days (168 hours) (Liu et al., 2022). The study by Liu et al. shows that after 7 days of incubation, the results for bacteria with nanometric polystyrene are similar to those without polymer. The publication described and compared groups of compounds, and we compared individual carbon sources. Our results indicate that for nanoPET, the differences in performance can be significant. Although the observed changes are complex, it can be assumed that the causes may be twofold, occurring simultaneously to varying degrees. First, nanoPETs may adsorb individual carbon sources, reducing their bioavailability. Second, nanoPET-induced oxidative stress may contribute to changes in metabolic pathways related to energy source metabolism and EPS formation, as described by Maksimova et al. in the case of carbon nanotube interaction with *E. coli* (Maksimova et al., 2023).

The presence of nanoPETs affected the permeability of the cell membranes of the strains tested. Analysing the effect of the tested nanoPETs on the *Bacillus* strain, it can be concluded that only nanoPET+Eu(TTA)$_3$ at concentrations greater than or equal to 50 μg/mL contributed to a decrease in cell membrane permeability as measured by the degree of crystal fillet penetration into the cells. At the same time, this nanoparticle had no effect on the cell membrane permeability of the *Lelliottia* strain, while in the case of the *Pseudomonas* strain, an increase in cell membrane permeability was observed in their presence, even at concentrations greater than or equal to 6.25 μg/mL. In contrast, the presence of nanoPETs and nanoPET+UCNPs only had an adverse effect on *Bacillus* β-galactosidase release from the cell. The observed effect may be due to nanoPET particles clogging pores in the *Bacillus* cell membrane. It is noteworthy that, despite the weaker permeability of the cell membrane, *Bacillus* released enough GST enzyme to detoxify the nanoPETs and multiply its abundance. This behaviour of the bacterial cells may be indicative of stress that the presence of nanoPETs may have caused. No studies were found on the effect of nanoPET on bacterial cell membrane permeability, but the work by Dai et al. (Dai et al., 2022) proved that positively charged nanoplastics up to 80 nm in diameter can penetrate the membrane.

AFM analysis showed that the obtained nanoPETs adsorbed on the surface of all three bacterial strains, forming long chains and clusters of nanoPET particles. To the best of our knowledge,

this publication presents the adhesion of nanoPET to bacterial cells using the AFM technique for the first time. Moreover, the presence of nanoPETs influences *Bacillus* biofilm formation. For each nanoPET, agglomerates can be seen on the surface of the *Bacillus* biofilms, which are not present when the bacteria are not exposed to the plastic. The number of agglomerates depends on the type of nanoPET used. Similarly, biofilm formation by *Lelliottia* also depends on the type of plastic used. From the photos (Figure 7), the biofilm had a different consistency in the company of labelled and unlabelled plastic and the control. The effect of nanoPETs on the formation of *Pseudomonas* biofilms was not proven. No studies of the impact of nanoPET on bacterial biofilm were found in the literature. However, the effect of nanometric polystyrene on biofilm formation by different bacterial species has been studied (Okshevsky et al., 2020). Okshevsky et al. showed that, depending on the bacterial species studied, the concentration of nanometric polystyrene could affect the formation of agglomerates by bacteria and the amount of biofilm they formed. Moreover, as Sun et al. noted, polystyrene nanoparticles caused oxidative stress and a cellular response characterized by increased EPS production (Sun et al., 2018). This may also explain the observed changes in biofilm production and the formation of agglomerates within it. This is most likely how the cells deactivated the nanoPET.

Bioimaging has proven that using nanoPET labelled with UCNPs is an effective and straightforward method to identify PET in bacterial biofilms. The photon upconversion phenomenon allows the detection of the emission of Er^{3+} ions without recording emission from bacterial proteins. According to a literature review, no one has previously studied bacteria with nanoPET-labeled UCNPs on a Labrox plate reader. However, a publication (Hosseinifard et al., 2024) describes imaging UCNPs in wheat. In the case of Eu^{3+}-labelled nanoPET, the usual fluorescence phenomenon is observed, which is also characteristic of bacterial proteins. For this reason, it was impossible to distinguish nanoPET+$Eu(TTA)_3$ from the bacterial biofilm, and it was necessary to dissolve the bacterial proteins. The emission intensity of nanoPET+$Eu(TTA)_3$ biofilm solutions showed no dependence on nanoPET+$Eu(TTA)_3$ concentration. These results show that labelling with Eu^{3+} ions does not give as good results as labelling with UCNPs. Nevertheless, it can also be used to label nanoPET, allowing estimation of its content in a biological sample.

5. Conclusions

The presented research has allowed us to evaluate the effect of nanoPET on environmental bacteria and has also shown that UCNPs, as well as $Eu(TTA)_3$, can be used as nanoplastic markers. During the study, suspensions of nanoPETs, both unlabelled and labelled, were successfully synthesised. Their luminescence characteristic shows that their emission maxima are at 660 and 612 nm, respectively. The labelled and non-labelled nanoPETs possessed analogous particle properties with a mean size below 145 nm. That allows us to conclude that the introduced markers do not significantly alter the properties of the synthesised nanoPET particles compared with unlabelled ones.

The collected data show that nanoPETs (both labelled and unlabelled) do not have a direct toxic effect on the cells of strains of the genera *Bacillus*, *Lelliottia,* and *Pseudomonas*. However, the nanoPETs affect their metabolism and also cause a decrease in glutathione S-transferase activity (by at least 15% for all strains), an enzyme involved in the cellular response to stress factors. Moreover, the nanoPET+UCNPs particles modified the permeability of the *Bacillus* cell membrane by nearly 50%, and one mechanism explaining this phenomenon is the adsorption

of the nanoplastic on the bacterial cell surface, as confirmed by AFM microscopy. Using markers, such as UCNPs, it was possible to visualize the nanoplastic sorption by the bacterial biofilm. Consequently, we confirmed that the proposed labelling techniques, particularly UCNPs, are a valuable tool for monitoring nanoPET, and, in addition, it was possible to collect a large dataset of information on the ecotoxicity of nanoPET against environmental bacteria belonging to three different genera.

The results suggest that PET nanoparticles, although relatively non-toxic, are a stress factor for microbial cells. At the same time, they can affect the metabolism and cellular properties of environmental bacteria, which have a key role in the natural metabolism cycle. Because nanoPET changes cell membrane permeability, the prevalence of nanoplastics may also change how bacteria interact with their environment, including other organisms and chemical compounds. Such changes may accumulate and lead to unpredictable consequences, e.g., in sewage treatment plants where biofilm is crucial for treatment efficiency.

Acknowledgements

This research was funded by the National Science Centre, Poland, with a grant number of 2022/45/B/ST5/00604.

We want to thank Oliwia Krysiak for her technical support in the laboratory work.

Author contributions

Klaudia Krysiak-Smułek: Conceptualization, Methodology, Formal analysis, Investigation, Writing - Original Draft, Visualization. **Wojciech Smułek:** Conceptualization, Methodology, Formal analysis, Investigation, Writing - Original Draft, Writing - Review & Editing, Visualization. **Dominika Przybylska:** Methodology, Formal analysis, Investigation, Writing - Original Draft, Visualization. **Zbigniew Hnatejko:** Methodology, Investigation, Writing - Original Draft. **Ewa Kaczorek:** Conceptualization, Resources, Writing - Review & Editing, Supervision. **Tomasz Grzyb:** Conceptualization. Methodology, Validation, Resources, Writing - Review & Editing, Supervision, Project administration, Funding acquisition.

References

Auzel, F., 2004. Upconversion and Anti-Stokes Processes with f and d Ions in Solids. Chem. Rev. 104, 139–174. https://doi.org/10.1021/cr020357g

Benyathiar, P., Kumar, P., Carpenter, G., Brace, J., Mishra, D.K., 2022. Polyethylene Terephthalate (PET) Bottle-to-Bottle Recycling for the Beverage Industry: A Review. Polymers 14, 2366. https://doi.org/10.3390/polym14122366

Binnemans, K., 2015. Interpretation of europium(III) spectra. Coord. Chem. Rev. 295, 1–45. https://doi.org/10.1016/j.ccr.2015.02.015

Bläsing, M., Amelung, W., 2018. Plastics in soil: Analytical methods and possible sources. Sci. Total Environ. 612, 422–435. https://doi.org/10.1016/j.scitotenv.2017.08.086

Brennetot, R., Georges, J., 2000. Investigation of chelate formation, intramolecular energy transfer and luminescence efficiency and lifetimes in the Eu–thenoyltrifluoroacetone–trioctylphosphine oxide–Triton X-100 system using absorbance, fluorescence and photothermal measurements. Spectrochim. Acta. A. Mol. Biomol. Spectrosc. 56, 703–715. https://doi.org/10.1016/S1386-1425(99)00175-4

Cortés-Arriagada, D., 2021. Elucidating the co-transport of bisphenol A with polyethylene terephthalate (PET) nanoplastics: A theoretical study of the adsorption mechanism. Environ. Pollut. 270, 116192. https://doi.org/10.1016/j.envpol.2020.116192

Dai, S., Ye, R., Huang, J., Wang, B., Xie, Z., Ou, X., Yu, N., Huang, C., Hua, Y., Zhou, R., Tian, B., 2022. Distinct lipid membrane interaction and uptake of differentially charged nanoplastics in bacteria. J. Nanobiotechnology 20, 191. https://doi.org/10.1186/s12951-022-01321-z

Devi, K.P., Sakthivel, R., Nisha, S.A., Suganthy, N., Pandian, S.K., 2013. Eugenol alters the integrity of cell membrane and acts against the nosocomial pathogen Proteus mirabilis. Arch. Pharm. Res. 36, 282–292. https://doi.org/10.1007/s12272-013-0028-3

Dhaka, V., Singh, S., Anil, A.G., Sunil Kumar Naik, T.S., Garg, S., Samuel, J., Kumar, M., Ramamurthy, P.C., Singh, J., 2022. Occurrence, toxicity and remediation of polyethylene terephthalate plastics. A review. Environ. Chem. Lett. 20, 1777–1800. https://doi.org/10.1007/s10311-021-01384-8

Djapovic, M., Apostolovic, D., Postic, V., Lujic, T., Jovanovic, V., Stanic-Vucinic, D., Van Hage, M., Maslak, V., Cirkovic Velickovic, T., 2023. Characterization of Nanoprecipitated PET Nanoplastics by 1H NMR and Impact of Residual Ionic Surfactant on Viability of Human Primary Mononuclear Cells and Hemolysis of Erythrocytes. Polymers 15, 4703. https://doi.org/10.3390/polym15244703

Djapovic, M., Milivojevic, D., Ilic-Tomic, T., Lješević, M., Nikolaivits, E., Topakas, E., Maslak, V., Nikodinovic-Runic, J., 2021. Synthesis and characterization of polyethylene terephthalate (PET) precursors and potential degradation products: Toxicity study and application in discovery of novel PETases. Chemosphere 275, 130005. https://doi.org/10.1016/j.chemosphere.2021.130005

European Commission. Directorate General for Environment., University of the West of England (UWE). Science Communication Unit., 2023. Nanoplastics: state of knowledge and environmental and human health impacts. Publications Office, LU.

Grzyb, T., Lis, S., 2011. Structural and Spectroscopic Properties of LaOF:Eu^{3+} Nanocrystals Prepared by the Sol–Gel Pechini Method. Inorg. Chem. 50, 8112–8120. https://doi.org/10.1021/ic2005453

Honselmann Genannt Humme, J., Dubrowska, K., Grygorcewicz, B., Gliźniewicz, M., Paszkiewicz, O., Głowacka, A., Musik, D., Story, G., Rakoczy, R., Augustyniak, A., 2024. Optimised stress – intensification of pyocyanin production with zinc oxide nanoparticles. Microb. Cell Factories 23. https://doi.org/10.1186/s12934-024-02486-y

Jannatin, M., Yang, T.-L., Su, Y.-Y., Mai, R.-T., Chen, Y.-C., 2024. Europium Ion-Based Magnetic-Trapping and Fluorescence-Sensing Method for Detection of Pathogenic Bacteria. Anal. Chem. 96, 5669–5676. https://doi.org/10.1021/acs.analchem.4c00655

Jin, B., Wang, S., Lin, M., Jin, Y., Zhang, S., Cui, X., Gong, Y., Li, A., Xu, F., Lu, T.J., 2017. Upconversion nanoparticles based FRET aptasensor for rapid and ultrasenstive bacteria detection. Biosens. Bioelectron. 90, 525–533. https://doi.org/10.1016/j.bios.2016.10.029

Johnson, L.M., Mecham, J.B., Krovi, S.A., Moreno Caffaro, M.M., Aravamudhan, S., Kovach, A.L., Fennell, T.R., Mortensen, N.P., 2021. Fabrication of polyethylene terephthalate (PET) nanoparticles with fluorescent tracers for studies in mammalian cells. Nanoscale Adv. 3, 339–346. https://doi.org/10.1039/D0NA00888E

Jurga, N., Przybylska, D., Kamiński, P., Tymiński, A., Grześkowiak, B.F., Grzyb, T., 2022. Influence of the synthesis route on the spectroscopic, cytotoxic, and temperature-sensing properties of oleate-capped and ligand-free core/shell nanoparticles. J. Colloid Interface Sci. 606, 1421–1434. https://doi.org/10.1016/j.jcis.2021.08.093

Jurga, N., Przybylska, D., Żychlińska, D., Grzyb, T., 2025. Upconversion luminescence in monoclinic $BaY_2F_8:Yb^{3+}$, Ln^{3+} (Ln = Er, Ho, Tm) nanoparticles synthesized by hydrothermal method. J. Alloys Compd. 1010, 178146. https://doi.org/10.1016/j.jallcom.2024.178146

Jurga, N., Ryszczyńska, S., Grzyb, T., 2023. Designing photon upconversion nanoparticles capable of intense emission in whole human blood. Spectrochim. Acta. A. Mol. Biomol. Spectrosc. 303, 123220. https://doi.org/10.1016/j.saa.2023.123220

Karkanorachaki, K., Tsiota, P., Dasenakis, G., Syranidou, E., Kalogerakis, N., 2022. Nanoplastic Generation from Secondary PE Microplastics: Microorganism-Induced Fragmentation. Microplastics 1, 85–101. https://doi.org/10.3390/microplastics1010006

Kohanski, M.A., DePristo, M.A., Collins, J.J., 2010. Sublethal Antibiotic Treatment Leads to Multidrug Resistance via Radical-Induced Mutagenesis. Mol. Cell 37, 311–320. https://doi.org/10.1016/j.molcel.2010.01.003

Liu, Y., Li, W., Tao, C., Zhao, J., Zhang, H., Miao, L., Pang, Y., Hou, J., 2022. Distinct Responses of Biofilm Carbon Metabolism to Nanoplastics with Different Surface Modifications. Int. J. Environ. Res. Public. Health 19, 9148. https://doi.org/10.3390/ijerph19159148

Maksimova, Y., Zorina, A., Nesterova, L., 2023. Oxidative Stress Response and E. coli Biofilm Formation under the Effect of Pristine and Modified Carbon Nanotubes. Microorganisms 11, 1221. https://doi.org/10.3390/microorganisms11051221

Mallah, M.H., Shemirani, F., Ghannadi Maragheh, M., 2008. Use of dispersive liquid-liquid microextraction for simultaneous preconcentration of samarium, europium, gadolinium and dysprosium. J. Radioanal. Nucl. Chem. 278, 97–102. https://doi.org/10.1007/s10967-007-7220-1

Mettenbrink, E.M., Yang, W., Wilhelm, S., 2022. Bioimaging with Upconversion Nanoparticles. Adv. Photonics Res. 3, 2200098. https://doi.org/10.1002/adpr.202200098

Misiak, M., Prorok, K., Bednarkiewicz, A., 2012. Biologiczne zastosowania nanoluminoforów domieszkowanych lantanowcami. Wiadomości chemiczne 66, 394–443.

Nwogu, C., Uche, R., Igbokwe, J.O., Okoronkwo, A.C., 2019. Design and Development of a Plastic Powder Processing Machine for Recycling Used Polyethylene Therephthalate. Machine Design 11, 47–52. https://doi.org/10.24867/MD.11.2019.2.47-52

Okshevsky, M., Gautier, E., Farner, J.M., Schreiber, L., Tufenkji, N., 2020. Biofilm formation by marine bacteria is impacted by concentration and surface functionalization of polystyrene nanoparticles in a species-specific manner. Environ. Microbiol. Rep. 12, 203–213. https://doi.org/10.1111/1758-2229.12824

Ortega, D.E., Cortés-Arriagada, D., 2023. Atmospheric microplastics and nanoplastics as vectors of primary air pollutants - A theoretical study on the polyethylene terephthalate (PET) case. Environ. Pollut. 318, 120860. https://doi.org/10.1016/j.envpol.2022.120860

Owen, M.M., Achukwu, E.O., Hazizan, A.M., Romli, A.Z., Ishiaku, U.S., 2022. Characterization of recycled and virgin polyethylene terephthalate composites reinforced with modified kenaf fibers for automotive application. Polym. Compos. 43, 7724–7738. https://doi.org/10.1002/pc.26866

Pacholak, A., Simlat, J., Zgoła-Grześkowiak, A., Kaczorek, E., 2018. Biodegradation of clotrimazole and modification of cell properties after metabolic stress and upon addition of saponins. Ecotoxicol. Environ. Saf. 161, 676–682. https://doi.org/10.1016/j.ecoenv.2018.06.050

Pallares, R.M., An, D.D., Hébert, S., Faulkner, D., Loguinov, A., Proctor, M., Villalobos, J.A., Bjornstad, K.A., Rosen, C.J., Vulpe, C., Abergel, R.J., 2021. Multidimensional genome-wide screening in yeast provides mechanistic insights into europium toxicity. Metallomics 13, mfab061. https://doi.org/10.1093/mtomcs/mfab061

Piccardo, M., Provenza, F., Grazioli, E., Cavallo, A., Terlizzi, A., Renzi, M., 2020. PET microplastics toxicity on marine key species is influenced by pH, particle size and food variations. Sci. Total Environ. 715, 136947. https://doi.org/10.1016/j.scitotenv.2020.136947

Pisarski, W.A., Pisarska, J., Lisiecki, R., Ryba-Romanowski, W., 2017. Erbium-doped lead silicate glass for near-infrared emission and temperature-dependent up-conversion applications. Opto-Electron. Rev. 25, 238–241. https://doi.org/10.1016/j.opelre.2017.06.011

Prabakaran, E., Pillay, K., 2020. Synthesis and characterization of fluorescent Europium (III) complex based on D-dextrose composite for latent fingerprint detection. J. Saudi Chem. Soc. 24, 584–605. https://doi.org/10.1016/j.jscs.2020.06.002

Przybylska, D., Jurga, N., Ekner-Grzyb, A., Stopikowska, N., Grześkowiak, B.F., Runowski, M., Grzyb, T., 2024. Optical Temperature Sensing and Bioimaging of Aquatic Invertebrates With Nd^{3+} - Sensitized Core@Shell Nanoparticles. Adv. Opt. Mater. 12, 2401499. https://doi.org/10.1002/adom.202401499

Sathicq, M.B., Sabatino, R., Di Cesare, A., Eckert, E.M., Fontaneto, D., Rogora, M., Corno, G., 2022. PET particles raise microbiological concerns for human health while tyre wear microplastic particles potentially affect ecosystem services in waters. J. Hazard. Mater. 429, 128397. https://doi.org/10.1016/j.jhazmat.2022.128397

Sharma, P., Kishore, A., Singh, M., 2024. Single-use polyethylene terephthalate bottle-derived nanoplastics propagate antibiotic resistance in bacteria *via* transformation and outer membrane vesicle secretion. Nanoscale 16, 21360–21378. https://doi.org/10.1039/D4NR02613F

Singh, A.K., Bedi, R., Kaith, B.S., 2021. Composite materials based on recycled polyethylene terephthalate and their properties – A comprehensive review. Compos. Part B Eng. 219, 108928. https://doi.org/10.1016/j.compositesb.2021.108928

Smułek, W., Pacholak, A., Kaczorek, E., 2020. Modification of the Bacterial Cell Wall—Is the Bioavailability Important in Creosote Biodegradation? Processes 8, 147. https://doi.org/10.3390/pr8020147

Smułek, W., Zdarta, A., Pacholak, A., Runka, T., Kaczorek, E., 2019. Increased biological removal of 1-chloronaphthalene as a result of exposure: A study of bacterial adaptation strategies. Ecotoxicol. Environ. Saf. 185, 109707. https://doi.org/10.1016/j.ecoenv.2019.109707

Sofo, A., Ricciuti, P., 2019. A Standardized Method for Estimating the Functional Diversity of Soil Bacterial Community by Biolog® EcoPlatesTM Assay—The Case Study of a Sustainable Olive Orchard. Appl. Sci. 9, 4035. https://doi.org/10.3390/app9194035

Sroczyńska, J., Guzik, U., Smułek, W., 2024. Permethrin Insecticide Influence on Microorganisms Present in Surface Waters. Appl. Sci. 14, 11589. https://doi.org/10.3390/app142411589

Sulyman, M., Haponiuk, J., Formela, K., 2016. Utilization of Recycled Polyethylene Terephthalate (PET) in Engineering Materials: A Review. Int. J. Environ. Sci. Dev. 7, 100–108. https://doi.org/10.7763/IJESD.2016.V7.749

Sun, G., Xie, Y., Sun, L., Zhang, H., 2021. Lanthanide upconversion and downshifting luminescence for biomolecules detection. Nanoscale Horiz. 6, 766–780. https://doi.org/10.1039/D1NH00299F

Sun, X., Chen, B., Li, Q., Liu, N., Xia, B., Zhu, L., Qu, K., 2018. Toxicities of polystyrene nano- and microplastics toward marine bacterium Halomonas alkaliphila. Sci. Total Environ. 642, 1378–1385. https://doi.org/10.1016/j.scitotenv.2018.06.141

Szczeszak, A., Ekner-Grzyb, A., Runowski, M., Szutkowski, K., Mrówczyńska, L., Kaźmierczak, Z., Grzyb, T., Dąbrowska, K., Giersig, M., Lis, S., 2016. Spectroscopic, structural and in vitro cytotoxicity evaluation of luminescent, lanthanide doped core@shell nanomaterials $GdVO_4:Eu^{3+}5\%@SiO_2@NH_2$. J. Colloid Interface Sci. 481, 245–255. https://doi.org/10.1016/j.jcis.2016.07.025

Würth, C., Grauel, B., Pons, M., Frenzel, F., Rissiek, P., Rücker, K., Haase, M., Resch-Genger, U., 2022. Yb- and Er concentration dependence of the upconversion luminescence of highly doped $NaYF_4$:Yb,Er/$NaYF_4$:Lu core/shell nanocrystals prepared by a water-free synthesis. Nano Res. 15, 9639–9646. https://doi.org/10.1007/s12274-022-4570-5